# Enzymatic oxidation of ansa-ferrocifen leads to strong and selective thioredoxin reductase inhibition in vitro

Valeria Scalcon, Anna Citta, Alessandra Folda, Alberto Bindoli, Michèle Salmain, Ilaria Ciofini, Sébastien Blanchard, José de Jesús Cázares Marinero, Wang Yong, Pascal Pigeon, et al.

HAL Id: hal-01401089

https://hal.sorbonne-universite.fr/hal-01401089v1

Submitted on 2 May 2018

# Enzymatic oxidation of ansa-ferrocifen leads to strong and selective

# thioredoxin reductase inhibition in vitro

Valeria Scalcon,[a] Anna Citta,[a] Alessandra Folda,[a] Alberto Bindoli,[b] Michèle Salmain,[c] Ilaria Ciofini,[d] Sébastien Blanchard,[c] José de Jesus Cazares-Marinero,[c] Yong Wang,[c,d] Pascal Pigeon,[c,d] Gérard Jaouen,[c,d] Anne Vessières,[c]* Maria-Pia Rigobello[a]*

a) Dipartimento di Scienze Biomediche, Università di Padova, Via Ugo Bassi 58/b, 35131 Padova, Italy

b) Istituto di Neuroscienze (CNR) Sezione di Padova, c/o Dipartimento di Scienze Biomediche, Via Ugo Bassi, 58/b, 35131 Padova, Italy

c) Sorbonne Universités, UPMC Univ Paris 06, CNRS, Institut Parisien de Chimie Moléculaire (IPCM), 75005 Paris, France

d) PSL Research University, Chimie ParisTech, 11 rue Pierre et Marie Curie, 75005 Paris, France

* Maria-Pia Rigobello and Anne Vessières, co-corresponding authors

## Abstract

This paper reports the inhibitory effect on the cytosolic thioredoxin reductase (TrxR1) in vitro by the ansa-ferrocifen derivative (ansa-FcdiOH, **1**). We found that **1** decreased only slightly enzyme activity (IC$_{50}$ =8 μM), while **1**$^*$, the species generated by enzymatic oxidation by the HRP (horseradish peroxidase)/H$_2$O$_2$ mixture, strongly inhibited TrxR1 (IC$_{50}$ = 0.15 μM). At the same concentrations, neither **1** nor **1**$^*$ had effect on glutathione reductase (GR). The most potent TrxR1 inhibitor did not appear to be the corresponding quinone methide as it was the case for ferrocifens of the acyclic series, or the stabilized carbocation as in the osmocifen series, but rather  the quinone methide radical. This hypothesis was confirmed by

ab-initio calculations of the species generated by oxidation of **1** and by EPR spectroscopy. BIAM (biotin-conjugated iodoacetamide) assay showed that **1**[*] targeted both cysteine and selenocysteine of the C-terminal redox center of TrxR1.

## 1. Introduction

As part of the search for new metallodrugs, ferrocene (Fc) derivatives have been widely explored and display contrasting antiproliferative effects while relatively few mechanistic pathways have as yet become clear [1–3]. We have ourselves synthesized derivatives of phenols, collectively called ferrocifens bearing an Fc-type redox antenna and an intramolecular electronic connection afforded by an olefin group (Chart S1) [3,4]. In the acyclic series the $IC_{50}$ values obtained on cancer cells for ferrocenyl mono, diphenol and tamoxifen like are in the order of 0.5 μM on MDA-MB-231 human breast cancer cells [5,6].

Complementary studies showed that oxidation of the [ferrocene-ene-phenol] motif gives rise to relatively stable yet electrophilic quinone methide (QM) metabolites via a mechanism involving the abstraction of 2 electrons and 2 protons [7–9]. These molecules were shown to react with thiols via a 1,8-Michael addition [10,11]. With the aim of enhancing the cytotoxic character of ferrocifens, the ansa-FcdiOH **1** was prepared [12,13] and formulated for in vivo studies [14]. It is three to five times more active than the ferrocifens of the acyclic series with $IC_{50}$ value down to 0.09 μM on MDA-MB-231 cell line. Up to now we have not been able to settle whether the complexes of the acyclic and ansa series acted via the same mechanism of action or not [15,16].

Many cytotoxic compounds, and in particular organometallic complexes such as *N*-heterocyclic carbene (NHC) gold complexes, are strong inhibitors of thioredoxin reductases (TrxRs), selenoenzymes involved in cellular redox regulation [17]. Both cytosolic and mitochondrial thioredoxin reductase isoforms possess a C-terminal active site containing a selenocysteine residue with a low pKa [18,19] therefore endowed with enhanced nucleophilicity. Consequently, many compounds, including anticancer agents, are considered to effectively target TrxR. Knowing the strong inhibiting properties of both electrophiles and metal complexes, we recently investigated the inhibitory properties of ferrocifens and osmocifens (Chart S1) and their QMs towards both isoforms of TrxR [10,20]. As expected, the

QMs were much stronger inhibitors than the parent compounds ($IC_{50}$ around 2.5 and 15 μM, for the ferrocifens and osmocifens respectively) [10]. We also showed that mild enzymatic oxidation of the ferrocifens by the $HRP/H_2O_2$ system generated species with the same spectral features as the authentic QMs. On the contrary, enzymatic oxidation of the osmocifens gave rise to different species that were identified as quinone methide cations and that displayed higher inhibitory properties towards TrxR than the QMs [20]. Thus, the species responsible for TrxR inhibition seems associated with different structures related to QMs. This prompted us to study the inhibitory effect of **1** on cytosolic TrxR [16]. Conversely to the acyclic ferrocifens and osmocifens, no quinone methide could be isolated from chemical oxidation of **1** [12]. This finding was ascribed to the constraints associated with its ansa structure that made the QM too unstable. Therefore, in the present paper, the enzymatic oxidation of **1** by the $HRP/H_2O_2$ system was investigated as well as the inhibitory effect of the resulting species on TrxR1. This hypothesis was substantiated by ab-initio calculations and EPR spectroscopy studies of the intermediate species generated by oxidation allowing assignment of the active species to a radical.

## 2. Materials and methods

Ansa-FcdiOH **1** was synthesized as previously described [12]. Stock solution ($1 \times 10^{-2}$ M) was prepared in DMSO and was stable for at least two months if kept at 4 °C. Horseradish peroxidase (HRP) and yeast glutathione reductase were purchased from Sigma Aldrich.

### 2.1 Enzymatic oxidation of *1* by the $HRP/H_2O_2$ system

Enzymatic oxidation of **1** (50 μM) by HRP (46 nM) and $H_2O_2$ (200 μM) was performed at pH 8.1 (0.2 M Tris HCl, 1 mM EDTA) or pH 5.0 (48.5 mM citric acid and 103 mM Na phosphate dibasic) containing 10% DMSO. HRP (40 μl of 1.14 μM solution) and $H_2O_2$ (20 μl of 10 mM solution) were pre-incubated for 5 min then added to the solution of **1** (940 μl). The solution was immediately transferred to a cuvette and the UV–Vis spectrum was recorded between 250 and 700 nm every 30 s on a Cary 50 spectrometer (Varian-Agilent, Santa Clara, CA, U.S.A.). Rate constants ($k_{obs}$) and half-lives ($t_{1/2}$) were calculated by fitting the $OD_{560\ nm}$ (at pH 8.1) or $OD_{413\ nm}$ (at pH 5) versus time data according to the first order law Eq. (1) with

Kaleidagraph software.

$$OD = C_0 + C1 \times \exp(-k_{obs} \times t) \qquad (1)$$
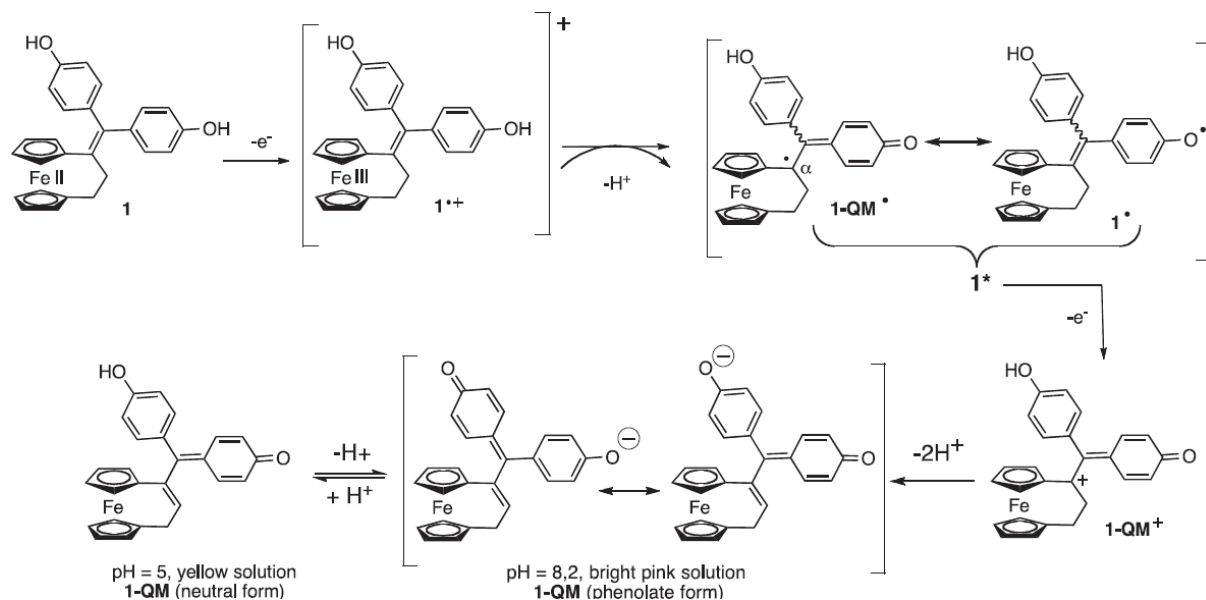


**Scheme 1.** Proposed oxidation sequence of **1** involving abstraction of 2 electrons and 3 protons and leading to the quinone methide (**1-QM**) followed by acid-base equilibrium of **1-QM**.

## 2.2 Computational details

All calculations were performed using the Gaussian09 software (cf. Supplementary information). All compounds reported in **Scheme 1** were optimized in the gas phase at Density Functional Theory level using the global hybrid PBE0 functional [21] and a double zeta basis set (including the corresponding pseudopotential to describe the core electrons of the metal atom [22]). The nature of each stationary point (i.e. minima) was confirmed by subsequent harmonic frequency calculations performed at the same level of theory. Calculations for open shell species were performed with an unrestricted formalism and spin polarization was found to be negligible. Vertical electronic transitions were computed using the optimized structures at TD-DFT level of theory using the same functional (PBE0) and a more extended basis (i.e. the 6–31 g(d) basis) set for all atoms but iron.

## 2.3 EPR spectroscopy studies

X-band EPR spectra were recorded on a Bruker Elexsys 500 spectrometer equipped with an Oxford Instrument continuous-flow liquid helium cryostat and a temperature control system.

A series of samples of **1** (50 µM) was mixed with HRP and $H_2O_2$ in buffer pH 8.1 as indicated in Section 2.1, transferred in quartz tubes and incubated for different times (1, 2, 5, 10 min). At the end of the incubation the tubes were frozen in a liquid nitrogen bath and introduced in the EPR cavity. EPR experiments were performed at 10 K, using a microwave power of 0.159 mW (non saturating conditions) with a modulation of 1 G.

*2.4 Thioredoxin reductase and glutathione reductase activity*

Complex **1** (0.25 µM) was pre-incubated for different times (0.5–60 min) with HRP/$H_2O_2$ (22 nM/0.1 mM) mixture giving **1**$^*$. At the end of the incubation period, aliquots of highly purified TrxR1 (60 nM), prepared as described previously [23], were preincubated with the compound for 5 min at 25 °C in 0.2 M Tris-HCl buffer (pH 8.1), 1 mM EDTA, and 0.25 mM NADPH. The reaction was started with 1 mM DTNB and followed spectrophotometrically at 412 nm for about 10 min.

GR activity (yeast glutathione reductase) was measured in 0.2 M Tris-HCl buffer (pH 8.1), 1 mM EDTA, and 0.25 mM NADPH after 5 min of preincubation with the various compounds (**1** or **1**$^*$). The assay was initiated by addition of 1 mM GSSG and followed spectrophotometrically at 340 nm.

*2.5 BIAM (biotinylated iodoacetamide) assay*

TrxR (1 µM), pre-reduced with NADPH (60 µM) in 50 mM Tris-HCl buffer (pH 7.4) containing 0.2 mM NADPH and 1 mM EDTA, was incubated for 30 min with 50 µM of **1** or 2 µM of **1**$^*$ (prepared as described in Section 2.1). Then, aliquots (8 µl) of the reaction mixture were added to 50 µM biotinylated iodoacetamide (BIAM) in either buffer at pH 6 (0.1 M HEPES-Tris) or pH 8.5 (0.1 M Tris-HCl) and incubated at room temperature for 30 min to alkylate the remaining –SH and/or SeH groups. Then the samples were subjected to SDS-PAGE onto Bis-Tris Gel NUPAGE (12%) (Life Technologies Corporation, Carlsbad, CA, U.S.A.)

and transferred to a nitrocellulose membrane. Proteins labeled with BIAM were detected with horseradish peroxidase-conjugated streptavidin and enhanced chemiluminescence detection [24].

## 3. Results and discussion

### 3.1 Kinetics of enzymatic oxidation of **1** by the HRP/H2O2 mixture at pH 8.1

Kinetics of enzymatic oxidation of **1** by HRP/$H_2O_2$ mixture was performed at pH 8.1, the pH used for the TrxR1 inhibition experiments, with a final concentration of 10% DMSO. Time evolution of the UV–Vis spectrum of **1** is shown in Fig. 1.
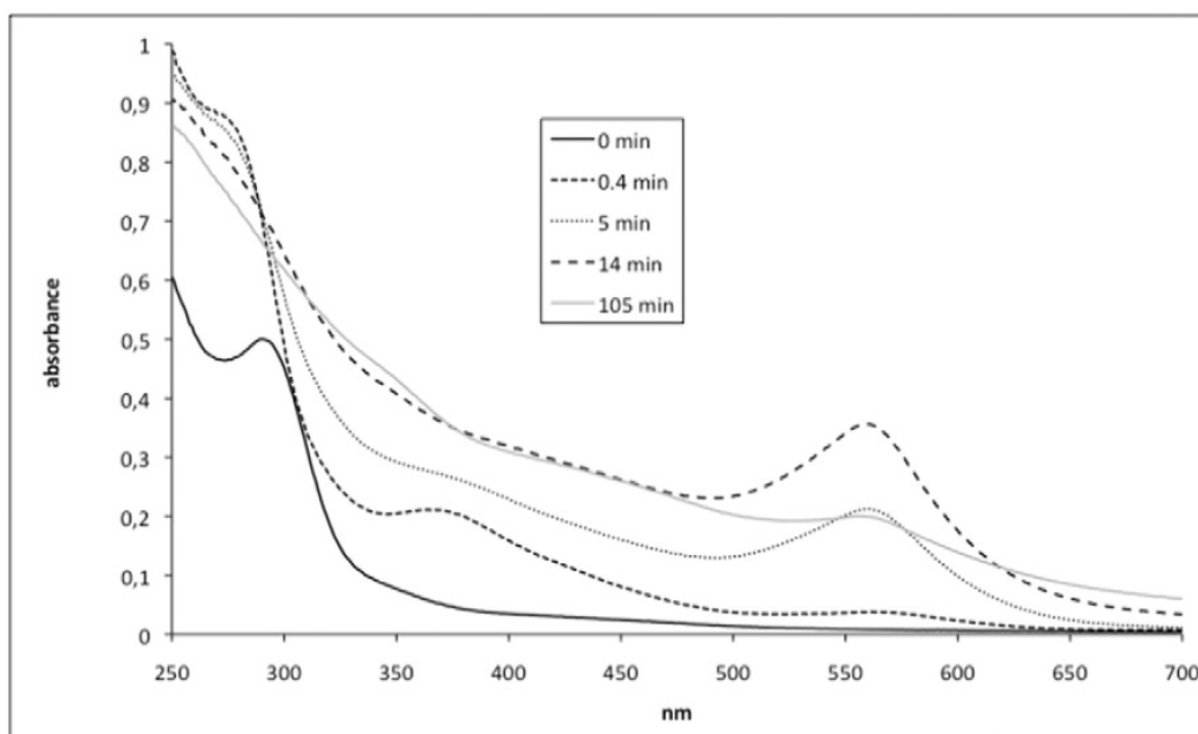


**Fig. 1.** Time evolution of the UV–Vis spectrum of **1** (50 μM) incubated at 25 °C in the presence of HRP (46 nM)/$H_2O_2$ (200 μM) at pH 8.1 (0.2 M Tris-HCl, 1 mM EDTA) containing 10% DMSO. Pure **1** (0 min): band at 291 nm; after 0.4 min: bands at 368 nm (broad) and 273 nm (shoulder); after 5 min and 14 min: band at 560 nm; after 105 min: significant decrease of the band at 560 nm.

We first observed the rapid appearance of two short-lived bands at 368 and 273 nm, only visible on the first spectrum recorded 0.4 min after addition of HRP + $H_2O_2$. It seems plausible to hypothesize that the structure of this transient species may be the radical $1^{\bullet}$ resulting from one electron oxidation and one proton abstraction of **1** (Scheme 1). This hypothesis was confirmed by DFT calculation and EPR spectroscopy of the species generated by oxidation of **1** (cf. Section 3.2).

Decreasing of these bands was followed by the emergence of a band at 560 nm associated with the bright pink color of the solution. The intensity of this band reached a maximum of absorbance at 15 min ($k_{obs} = 0.11 \pm 0.01$ min$^{-1}$, Fig. S1 A) then rapidly decreased ($t_{1/2} = 8$ min; $k_{obs} = 0.09$ min$^{-1}$, Fig. S1 B). This second species was attributed to the phenolate form of **1-QM** (Scheme 1).

This assignment was done by analogy with the spectral features of phenol red, the pH indicator classically used in cell culture, which also possesses a quinone methide – phenol motif (Fig. S2) and displays a bright pink color at pH 8.0 and a yellow color at pH 6.0. Actually, the $pK_a$ value of a phenol belonging to a quinone methide – phenol motif is equal to 8.0, a value significantly lower than that of phenol that is equal to 9.9. Thus, at pH 8.1 this phenol is mostly in its phenolate form. Its negative charge is delocalized and is at the origin of the observed bright pink color ($\lambda_{max} = 560$ nm) (Scheme 1). Indeed when enzymatic oxidation of **1** by the HRP/$H_2O_2$ mixture was carried out at pH 5.0, the solution turned yellow instead of pink (Table S1 and Fig. S3). This yellow color ($\lambda_{max} = 413$ nm) is the signature of the neutral quinone methide [10,25].

On the contrary to what is observed with phenol red, **1-QM** in its phenolate form was not stable, since gradual conversion of the pink color to brownish was observed with time along with the appearance of insoluble species, associated with an increase of the baseline.

*3.2 Nature of the intermediate species*

*3.2.1 Insights from DFT calculations*

The nature of the intermediate species reported in **Scheme 1** was further studied by ab-initio calculations performed at Density Functional Theory (DFT) level. As depicted in Fig. S4, collecting the computed spin density for the radical cation, $1^{\bullet+}$ and the radical $1^*$ species,

calculations unambiguously show that the first oxidation occurs at the Fe(II) center giving rise to a Fe(III) radical species ($\mathbf{1}^{\bullet+}$, Scheme 1). After deprotonation on the other hand, the unpaired electron of the neutral radical $\mathbf{1}^{*}$ is delocalized between the Cα position and the deprotonated phenol ring, so that two resonant structures can be formally written for this radical ($\mathbf{1}^{\bullet}$ and $\mathbf{1\text{-}QM}^{\bullet}$). The presence of this electron delocalization justifies the radical stability. Of note, the deprotonation of the two phenols is predicted to be practically isoenergetic (energy difference of 0.8 kcal/mol in the gas phase). The first oxidation, leading to the formation of the $\mathbf{1}^{\bullet+}$ species, is predicted to be more easily achievable than the second one yielding to the formation of the carbocationic species $\mathbf{1\text{-}QM}^{+}$ (energy difference of 6 kcal/mol) thus further substantiating the possibility of trapping the radical intermediate $\mathbf{1}^{*}$.

Determination of the structure of the transient species depicted on Fig. 1 (UV−Vis bands at 368 and 273 nm) is difficult to be experimentally achieved but, on the basis of the UV−Vis spectra computed at Time Dependent DFT (DFT) level, it is plausible to attribute it to $\mathbf{1}^{\bullet}$, the radical obtained after one electron oxidation and one proton abstraction of $\mathbf{1}$ (Scheme 1). Indeed, only for this species two electronic transitions are computed at 398 nm and 345 nm which give rise to the experimentally observed broad and asymmetric band observed at 368 nm. On the other hand all other plausible intermediates such as the $\mathbf{1}^{\bullet+}$ radical or the doubly oxidized carbocationic species ($\mathbf{1\text{-}QM}^{+}$) are predicted to have no electronic excitation in this spectral region and to absorb around 458 nm and 461 nm, respectively. Since no raise of bands is observed in this spectral region we can thus confidently assign the transient species to the $\mathbf{1}^{\square}$ radical. For the sake of completeness the full list of the electronic excitations computed for $\mathbf{1}$, $\mathbf{1}^{\bullet+}$, $\mathbf{1}^{\bullet}$ and $\mathbf{1\text{-}QM}^{+}$ are reported in Supplementary Information (Table S2).

### 3.2.2 Insights from EPR spectroscopy

EPR spectroscopy studies were performed to confirm the radical nature of $\mathbf{1}^{*}$. EPR spectrum recorded at 10 K after a 2 min period of incubation of $\mathbf{1}$ in the presence of HRP/$H_2O_2$ in buffer pH 8.1, clearly showed a sharp peak at g = 2.0205 characteristic of an organic radical (Fig. 2A) which is not visible on the spectrum of the control experiment (Fig. 2B).

Kinetic studies in the range 1−10 min showed that this peak reached a maximum after 2 min then slowly decreased but remained detectable after 10 min (Fig. S5). Thus, the formation of a

transient, but observable, organic radical species $1^*$ was confirmed by EPR spectroscopy.
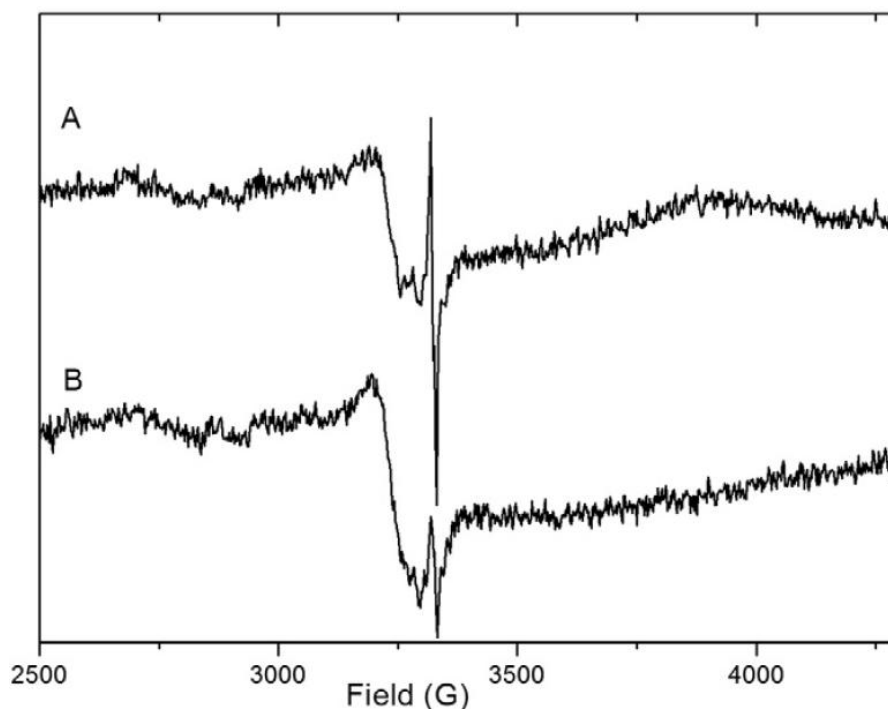


**Fig. 2.** EPR spectra recorded at 10 K at 9.3944 GHz of frozen solutions. A: spectrum after a 2 min incubation of **1** (50 μM) in the presence of HRP (46 nM)/$H_2O_2$ (200 μM) in buffer pH 8.1; B: spectrum of the control (HRP (46 nM)/$H_2O_2$ (200 μM) in buffer pH 8.1).

*3.3 Kinetics of inhibition of cytosolic thioredoxin reductase (TrxR1) in vitro by $1^*$, the enzymatically oxidized derivative of 1*

In our studies recently performed in the ferrocifen and osmocifen series, we observed that the parent complexes were always poor inhibitors of TrxRs while their QMs or the compounds obtained by enzymatic oxidation were strong inhibitors of their activity [10,20]. This inhibiting property was assigned to the Michael acceptor character of the QMs. As the synthesis of **1-QM** by chemical oxidation was unsuccessful [12], we decided to first study the kinetics of inhibition of TrxR1 by the compound(s) obtained by enzymatic oxidation of **1**. As enzymatic oxidation of **1** by the HRP/$H_2O_2$ mixture leads to short-lived compounds (vide supra), the activity of TrxR in the presence of $1^*$ was measured after short pre-incubation times (0.5–60 min) of **1** and HRP + $H_2O_2$. Results are displayed in Fig. 3.

The enzymatic activity of the mixtures of TrxR1 and enzymatically oxidized **1** was highly dependent on the time during which **1** and HRP + $H_2O_2$ were pre-incubated. It

decreased between 0.5 and 5 min pre-incubation time and reached a minimum (14% of residual activity) at 5 min. Thus the active species responsible for this rapid and efficient inactivation of TrxR1 may be attributed to $1^{\bullet}$ as this radical species is generated in this range of time and is supposed to be very reactive. The activity increased back for longer pre-incubation times, i.e. when **1-QM** is formed. It means that **1-QM** is a less potent inhibitor of TrxR1 than $1^{*}$. This lower reactivity of **1-QM** which is in its phenolate form at pH 8.1, could result from its delocalized charge and thus its lower electrophilicity.
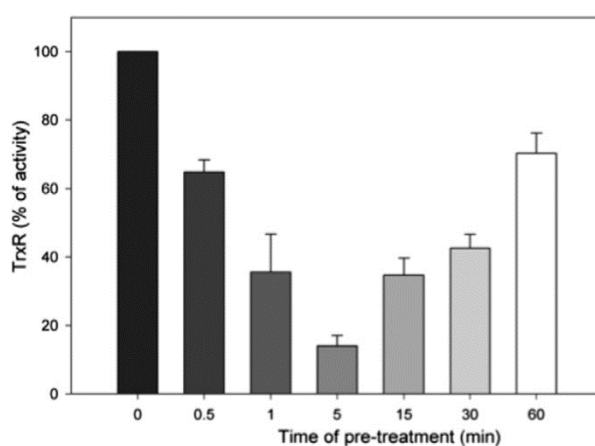


**Fig. 3.** Kinetics of inhibition of cytosolic thioredoxin reductase (TrxR1) in vitro by $1^{*}$, the enzymatically oxidized derivatives of **1**. Complex **1** (0.25 μM) was first preincubated for different times (0.5–60 min) with HRP/$H_2O_2$ (22 nM/0.1 mM) mixture giving $1^{*}$. At the end of the incubation, aliquots of highly purified TrxR1 (60 nM) prepared as described previously [23], in 0.2 M Tris-HCl, 1 mM EDTA buffer (pH 8.1) and NADPH (0.25 mM) were added and incubated for 5 min. Percentage of remaining TrxR1 activity was determined by estimating the DTNB-reducing property of the enzyme using a 1 mM DTNB solution monitored by UV–Vis at 412 nm for about 10 min.

*3.4 Inhibitory effect on cytosolic thioredoxin reductase (TrxR1) and glutathione reductase (GR) of **1** and of its enzymatically oxidized derivative ($1^{*}$)*

The inhibitory effect on TrxR1 and GR of various concentrations of **1** and of $1^{*}$, the oxidized species obtained after 5 min preincubation in the presence of the HRP/$H_2O_2$ mixture, was studied and the results shown in Fig. 4. GR also belongs to the family of pyridine nucleotide-disulfide oxidoreductases and is structurally homologous to TrxR except that it lacks the C-terminal redox center.
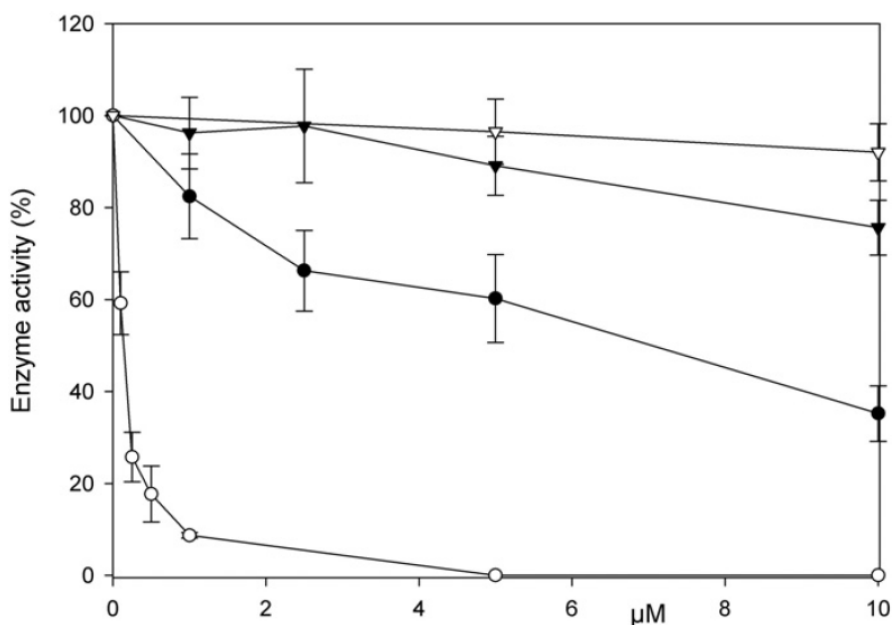
**Fig. 4.** Percentage of TrxR1 and of GR activities. Enzymes were incubated for 5 min in the presence of various concentrations of **1** (TrxR ●; GR ▼) or **1**$^*$ (TrxR ○; GR ∇). The latter was obtained by pretreatment of **1** with $H_2O_2$/HRP for 5 min as indicated in Materials and methods. TrxR1 and GR activities were measured as described in Materials and methods.

None of these species induced a significant inhibition of GR. Regarding TrxR1, **1** alone inhibited only slightly TrxR1 ($IC_{50}$ around 7 μM) while a significantly lower $IC_{50}$ value (around 0.15 μM) was found for the oxidized compound **1**$^*$. In the open series, QMs were also found to inhibit cytosolic and mitochondrial TrxR more efficiently than their parent compounds [10]. However, the $IC_{50}$ value found for **1**$^*$, hypothesized to be the quinone methide radical, was around ten times lower than that in the ferrocifen open series ($IC_{50}$ = 2.6 μM for Fc-monoOH-QM) [10]. This observation is fully consistent with our hypothesis that enzymatic oxidation of **1** leads to **1**$^{\bullet}$ that is expected to be more reactive than the anionic QM (see above). Interestingly, **1** was found to be significantly more cytotoxic on cancer cells than Fc-monoOH ($IC_{50}$ = 0.09 μM versus 1.5 μM on MDA-MB-231 breast cancer cells) [16]. Thus inhibition of TrxR1 could be a major target for expression of cytotoxicity of **1**. Moreover, the complete lack of activity of **1** and **1**$^*$ towards GR indicates that these complexes probably target the highly accessible C-terminal redox center of TrxR comprising Cys497 and Sec498.

*3.5 Interaction of **1** and **1**$^*$ with TrxR: BIAM assay*

In order to get information on the status of the C-terminal redox active center of reduced TrxR1 treated by **1** or **1**$^*$, a BIAM (biotin-conjugated iodoacetamide) assay was

performed. BIAM can alkylate TrxR1 by reaction of the thiol groups and/or the selenol group of Sec498 in a pH-dependent fashion. At pH 6, only selenocysteine can be derivatized, while at pH 8.5, both selenocysteine and cysteines can be derivatized by BIAM [24]. For this experiment, TrxR1 was first incubated with **1** and **1**[*]. Then the amounts of free selenocysteine and cysteine residues remaining on TrxR were quantified by reaction with BIAM at pH 6 or 8.5 followed by SDS-PAGE and detection of biotinylated protein with streptavidin-HRP. The corresponding Western Blot is displayed in Fig. 5.

Concerning **1**, no decrease of the band intensity was observed after reaction of BIAM at pH 6 (lane b), while a slight decrease was observed at pH 8.5 (lane b'). Thus **1**, at relatively high concentration (50 μM) is able to faintly interact with thiols, but is not related with the selenocysteine. Concerning **1**[*], at low concentration (2 μM), as reported in Fig. 5 lane c and c', is able to titrate selenocysteine and in addition to interact with thiols. As control, the mixture of $H_2O_2$/HRP alone is unable to affect TrxR1. These results are in good agreement with the respective potency of **1** and **1**[*] as TrxR inhibitors (low for **1**, high for **1**[*]; Fig. 5). Interestingly, this result differs from that previously observed for ferrocifens since they selectively reacted with the selenol group of Sec498 [10].
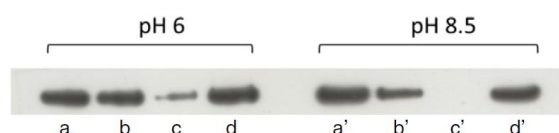


**Fig. 5.** Western Blot obtained after treatment of TrxR with **1** or **1**[*] followed by detection of the unreacted thiol/selenol residues by BIAM assay. TrxR1 (1 μM), pre-reduced with NADPH (60 μM), was incubated for 30 min with 50 μM of **1** or 2 μM of **1**[*] (prepared as described in Materials and methods) in 50 mM Tris-HCl buffer (pH 7.4) containing 0.2 mM NADPH, 1 mM EDTA. Then, aliquots (8 μl) of the reaction mixture were added to 50 μM biotinylated iodoacetamide (BIAM) in either buffer at pH 6 (0.1 M HEPES-Tris) or pH 8.5 (0.1 M Tris-HCl) and incubated at room temperature for 30 min to alkylate the remaining–SH–SeH groups then subjected to SDS-PAGE as described in ref. [24]. Lane a, a': control; lane b, b' 50 μM **1**; c, c' 2 μM **1**[*]; d, d' control with $H_2O_2$/HRP.

## 4 Conclusion

In the same experimental conditions of enzymatic oxidation by the HRP/$H_2O_2$ mixture previously used for metallocifens [10,20], we observed with **1**, transient short-lived species attributed to a radical (**1**[*]) that converted into an unstable quinone methide in neutral or anionic form depending on the pH. Even if the half-life of **1**[*] is short it is observable by UV–Vis and EPR

spectroscopies. This is attributed to the possibility of delocalization of the unpaired electron of $1^*$ between the C$\alpha$ position and the deprotonated phenol ring. On the contrary, the quinone methide was the unique species observed after enzymatic oxidation of Fc-monoOH and Fc-OHTam suggesting a lower half-life of the corresponding radicals. On the whole, the work presented here shed light on the variety of reactive species involved in the mechanism of inactivation of TrxR by metallocifens, namely quinone methide for Fc-monoOH and Fc-OHTam, cationic species for osmocifens and radicals for ansa-FcdiOH. The next step will be to understand the mechanism by which the radical species inactivates TrxR at the molecular level and whereas this occurs in cells.

The formation of a free radical species opens interesting perspective regarding the potential effects of these compounds on cancer cell viability. In addition to the inhibition of thioredoxin reductase the free radical species formed after biological oxidation of the inactive parent compound may act on different cell targets. Of note, the maximum effect is elicited about 5 min from its formation, while, for larger times the effects markedly decrease, which is compatible with the action of a free radical species.

**Author contributions**

V. S., A. C. and A. F. performed enzyme inhibitor studies.

M. S. performed enzymatic oxidation studies and calculation of rate constants and participate in interpretation of the data.

I. C. performed and interpreted DFT calculations.

S. B. performed and interpreted EPR spectra.

J. J. C. M. initiated DFT calculations.

Y. W. contributed to elucidate the structure of intermediates.

P. P. synthesized complex **1**.

A. B. and G. J. contributed to suggestion, interpretation and fruitful in the discussion of the results.

A.V. and M. P. R. did the planning of the study, the final co-supervision of the work, the interpretation of the data, the coordination between all authors, wrote the main manuscript linking the sections together and the final editing submission. All authors reviewed the manuscript.

*Abbreviations*

ansa-FcdiOH   1,1′-{1-[1,1-bis(4-hydroxyphenyl)methylidene]trimethylene}ferrocene

BIAM          biotinylated iodoacetamide

DFT           Density Functional Theory

DMSO          dimethyl sulfoxide

DTNB          5,5′-dithiobis(2-nitrobenzoic acid)

EPR           Electron Paramagnetic Resonance

Fc-monoOH     1-(4-hydroxyphenyl)-1-(phenyl)-2-ferrocenyl-but-1-ene

Fc-OHTam      1-[4-(3-dimethylaminopropyloxy)phenyl]-1-(4-hydroxyphenyl)-2-ferrocenyl-1-but-1-ene

GR            glutathione reductase

GSSG          oxidized glutathione

HEPES         4-(2-Hydroxyethyl)piperazine-1-ethanesulfonic acid

HRP           horseradish peroxidase

QM            quinone methide

ROS           reactive oxygen species

SeCys         selenocysteine

SDS-PAGE      sodium dodecyl sulfate polyacrylamide gel electrophoresis

| SH | thiol groups |
| --- | --- |
| TrxR | thioredoxin reductase |

## Acknowledgements

## References

[1] S.S. Braga, A.M.S. Silva, Organometallics 32 (2013) 5626–5639.

[2] S. Daum, V.F. Chekhun, I.N. Todor, N.Y. Lukianova, Y.V. Shvets, L. Sellner, K. Putzker, J. Lewis, T. Zenz, I.A.M. de Graaf, G.M.M. Groothuis, A. Casini, O. Zozulia, F. Hampel, A. Mokhir, J. Med. Chem. 58 (2015) 2015–2024.

[3] G. Jaouen, A. Vessières, S. Top, Chem. Soc. Rev. 44 (2015) 8802–8817.

[4] A. Vessières, J. Organomet. Chem. 734 (2013) 3–16.

[5] A. Nguyen, A. Vessières, E.A. Hillard, S. Top, P. Pigeon, G. Jaouen, Chimia 61 (2007) 716–724.

[6] S. Top, A. Vessières, G. Leclercq, J. Quivy, J. Tang, J. Vaissermann, M. Huché, G. Jaouen, Chem. Eur. J. 9 (2003) 5223–5236.

[7] D. Hamels, P.M. Dansette, E.A. Hillard, S. Top, A. Vessières, P. Herson, G. Jaouen, D. Mansuy, Angew. Chem. Int. Ed. 48 (2009) 9124–9126.

[8] E.A. Hillard, A. Vessières, L. Thouin, G. Jaouen, C. Amatore, Angew. Chem. Int. Ed. 45 (2006) 285–290.

[9] P. Messina, E. Labbé, O. Buriez, E.A. Hillard, A. Vessières, D. Hamels, S. Top, G. Jaouen, Y.M. Frapart, D. Mansuy, C. Amatore, Chem. Eur. J. 18 (2012) 6581–6587.

[10] A. Citta, A. Folda, A. Bindoli, P. Pascal Pigeon, S. Top, A. Vessières, M. Salmain, G. Jaouen, M.P. Rigobello, J. Med. Chem. 57 (2014) 8849–8859.

[11] Y. Wang, M.-A. Richard, S. Top, P.M. Dansette, P. Pigeon, A. Vessières, D. Mansuy, G. Jaouen, Angew. Chem. Int. Ed. (2016), http://dx.doi.org/10.1002/ange.201603931, (in press).

[12] D. Plazuk, A. Vessières, E.A. Hillard, O. Buriez, E. Labbé, P. Pigeon, M.A. Plamont, C. Amatore, J. Zakrzewski, G. Jaouen, J. Med. Chem. 52 (2009) 4964–4967.

[13] M. Görmen, D. Plazuk, P. Pigeon, E.A. Hillard, M.A. Plamont, S. Top, A. Vessières, G. Jaouen, Tetrahedron Lett. 51 (2010) 118–120.

[14] A.-L. Lainé, A. Clavreul, A. Rousseau, C. Tétaud, A. Vessières, E. Garcion, G. Jaouen, L. Aubert, M. Guilbert, J.P. Benoit, R.A. Toillon, C. Passirani, Nanomedicine: NBM 10 (2014) 1667–1677.

[15] C. Bruyère, V. Mathieu, A. Vessières, P. Pigeon, S. Top, G. Jaouen, R. Kiss, J. Inorg. Biochem. 141 (2014) 144–151.

[16] M. Görmen, P. Pigeon, S. Top, E.A. Hillard, M. Huché, C.G. Hartinger, F. de Montigny, M.-A. Plamont, A. Vessières, G. Jaouen, ChemMedChem 5 (2010) 2039–2050.

[17] E. Schuh, C. Pfluger, A. Citta, A. Folda, M.P. Rigobello, A. Bindoli, A. Casini, F. Mohr, J. Med. Chem. 55 (2012) 5518–5528.

[18] R.E. Huber, R.S. Criddle, Arch. Biochem. Biophys. 122 (1967) 164–173.

[19] L. Johansson, G. Gafvelin, E.S.J. Arner, Biochim. Biophys. Acta 1726 (2005) 1–13.

[20] V. Scalcon, S. Top, H.Z.S. Lee, A. Citta, A. Folda, A. Bindoli, W.K. Leong, A. Vessières, G. Jaouen, M.P. Rigobello, J. Inorg. Biochem. 16 (2016) 296–304.

[21] C. Adamo, V. Barone, J. Chem. Phys. 110 (1999) 6158–6170.

[22] P.J. Hay, W.R. Wadt, J. Chem. Phys. 82 (1985) 270–283.

[23] M. Luthman, A. Holmgren, Biochemistry 21 (1982) 6628–6633.

[24] J.G. Fang, J. Lu, A. Holmgren, J. Biol. Chem. 280 (2005) 25284–25290.

[25] P.W. Fan, F. Zhang, J.L. Bolton, Chem. Res. Toxicol. 13 (2000) 45–52.

# Supplementary Information

**Chart S1. Ferrocifens and osmocifens**



M = Fe
Fc-monoOH : $R_1$ = OH, $R_2$ = H
Fc-diOH : $R_1$ = OH, $R_2$ = OH
Fc-OHTam : $R_1$ = OH, $R_2$ = O(CH$_2$)$_3$N(CH$_3$)$_2$
M = Os
Oc-monoOH : $R_1$ = OH, $R_2$ = H
Oc-diOH : $R_1$ = OH, $R_2$ = OH
Oc-OHTam : $R_1$ = OH, $R_2$ = O(CH$_2$)$_3$N(CH$_3$)$_2$

**A)**

**Appearance of the peak with λ_max = 560 nm**

50 μM DP1 + HRP + H₂O₂ (pH 8.1)



| y = m1 + m2*exp(m3*x) | | |
|---|---|---|
| | Value | Error |
| m1 | 0,45157 | 0,015376 |
| m2 | -0,43869 | 0,012871 |
| m3 | -0,11367 | 0,0083963 |
| Chisq | 0,00042335 | NA |
| R | 0,99864 | NA |
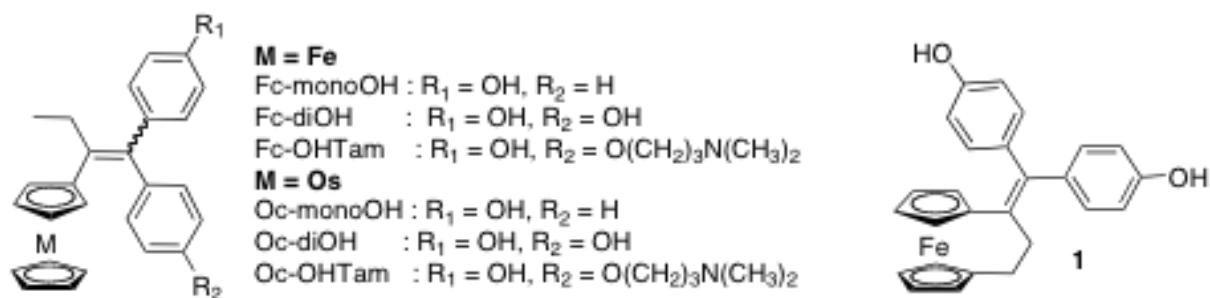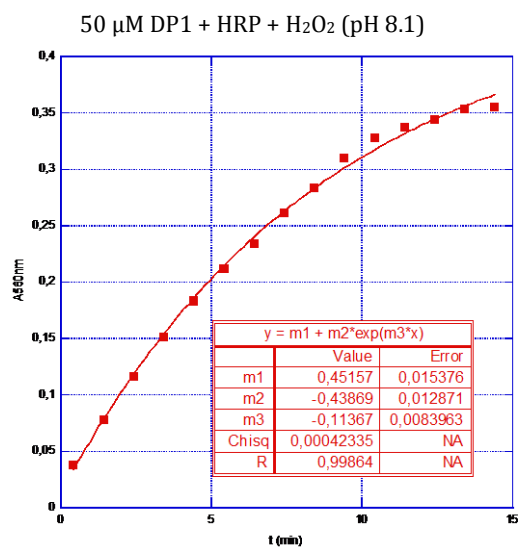
$k_{obs} = 0.11 \pm 0.01$ min$^{-1}$

**B)**

**Disappearance of the peak with λ_max = 560 nm**

50 μM DP1 + HRP + H₂O₂ (pH 8.1)



| y = m1 + m2*exp(-m3*x) | | |
|---|---|---|
| | Value | Error |
| m1 | 0,14348 | 0,00056204 |
| m2 | 0,25776 | 0,0041019 |
| m3 | 0,086522 | 0,0014745 |
| Chisq | 9,4951e-6 | NA |
| R | 0,9997 | NA |
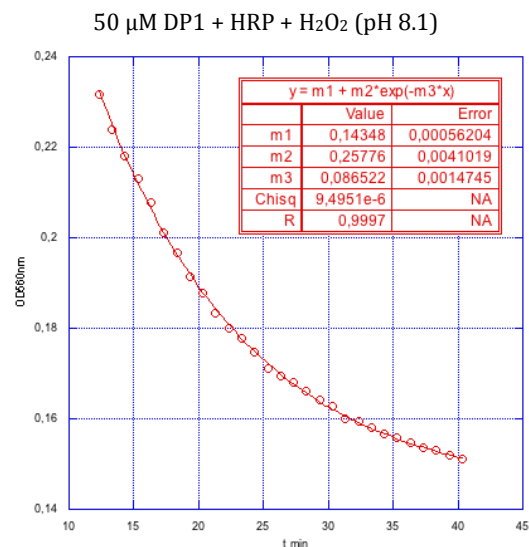
$k_{obs} = 0.09$ min$^{-1}$

$t_{1/2} = 8$ min

**C)**



before    53"    9'12"    19'50"    37'33"
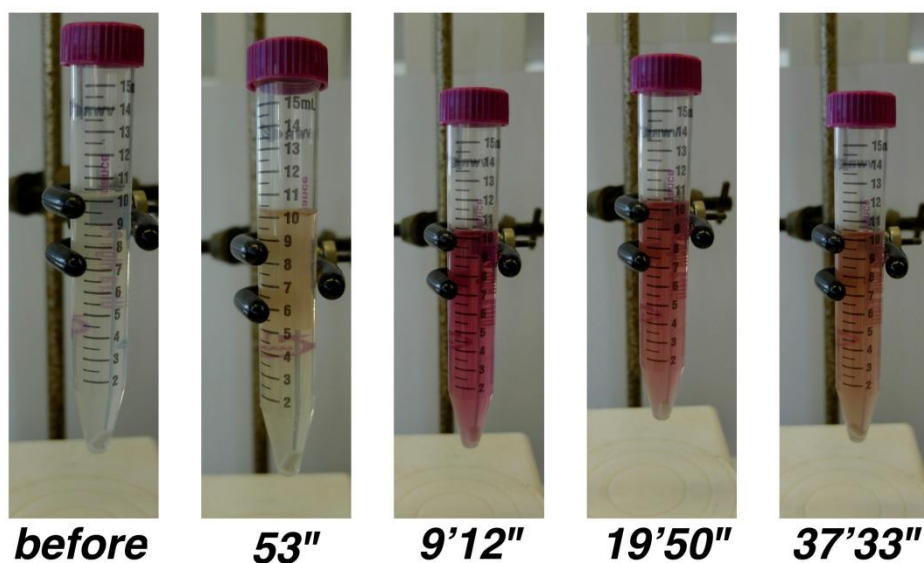
**Figure S1.** Measurement of the rate of enzymatic oxidation by HRP+H₂O₂ of **1** at pH 8.1. **A)** kinetics of formation of a species with λ_max = 560 nm in the range 0-14 min; **B)** kinetics of disappearance of this species in the range 15 – 120 min (experimental conditions [**1**] = 50 μM, [HRP] = 46 nM, [H₂O₂] = 200 μM in 0.2 M Tris-HCl (pH 8.1), 25°C containing 10% DMSO); C) pictures illustrating the color evolution of the reaction mixture (time between 0 and 37 min).

Yellow (pH = 5)                    Bright pink (pH = 8.1)

Phenolsulfonphatalein (phenol red)
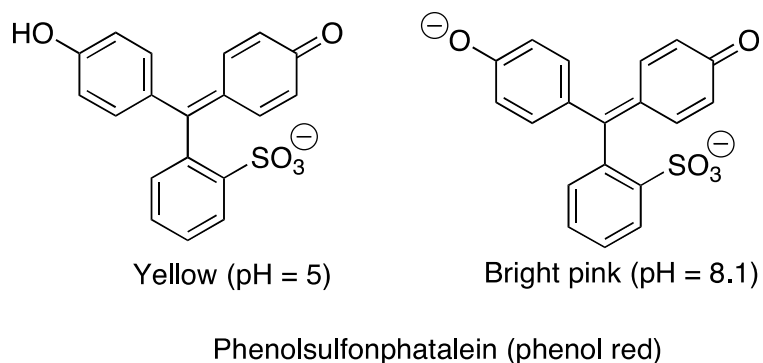
**Figure S2**. Chemical structure of phenol red at acidic and basic pH.

**Table S1**. Enzymatic oxidation of **1** (50 μM) by HRP (46 nM)/$H_2O_2$ (0.2 mM) system, kinetics of formation of the corresponding quinone methide under its phenolate form at pH 8.1 and neutral form at pH 5.0.

| pH 5.0 | pH 8.1 |
|---|---|
| color : yellow | color : pink , unstable species |
| $\lambda_{max}$ :413 nm, max at 10 min | $\lambda_{max}$ : 560 nm ; max at 15 min ; |
| Appearance : | Appearance : |
| $k_{obs}$ = 0.28 min$^{-1}$ | $k_{obs}$ = 0.11 min$^{-1}$ |
| Disappearance: | Disappearance : |
| $k_{obs}$ = 0.012 min$^{-1}$ | $k_{obs}$ = 0.043 min$^{-1}$ |
| $t_{1/2}$ = 58 min | $t_{1/2}$ = 16 min |
|  |  |
| **1-QM** under its neutral form | **1-QM** under its phenolate form |
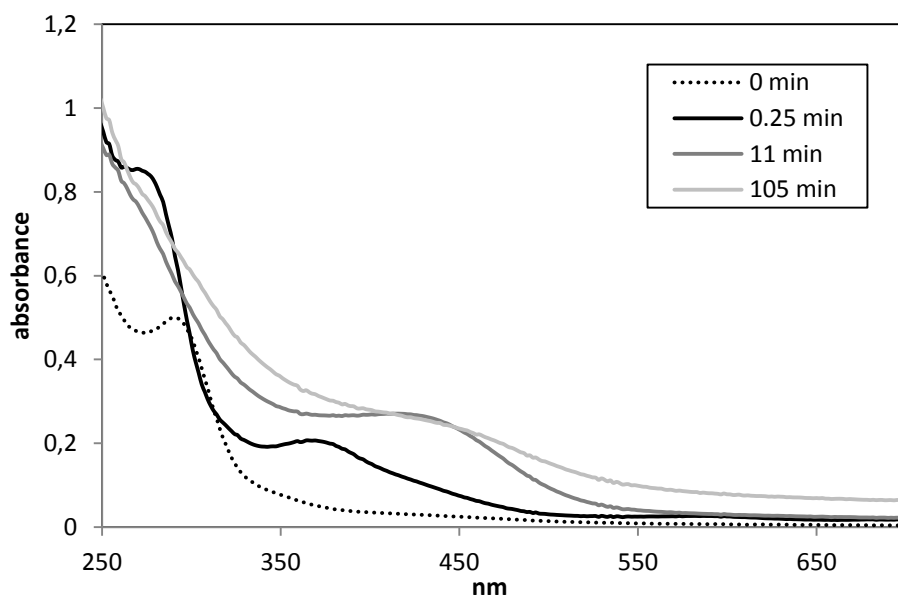
**Figure S3**. Time evolution of the UV-Vis spectrum of **1** (50 μM) incubated in the presence of HRP (46 nM) / $H_2O_2$ (200 μM) in citrate-phosphate buffer (48.5 mM citric acid and 103 mM Na phosphate dibasic pH 5.0) at 25°C. Pure **1** (0 min): band at 291 nm; after 0.25 min: bands at 369 nm (broad) and 273 nm; after 11 min: band at 413 nm; after 105 min flattening of the band at 413 nm.

**Computational Details**

All calculations were performed using Gaussian 09, Revision **A.02**, M. J. Frisch, G. W. Trucks, H. B. Schlegel, G. E. Scuseria, M. A. of the Gaussian09 software (Robb, J. R. Cheeseman, G. Scalmani, V. Barone, B. Mennucci, G. A. Petersson, H. Nakatsuji, M. Caricato, X. Li, H. P. Hratchian, A. F. Izmaylov, J. Bloino, G. Zheng, J. L. Sonnenberg, M. Hada, M. Ehara, K. Toyota, R. Fukuda, J. Hasegawa, M. Ishida, T. Nakajima, Y. Honda, O. Kitao, H. Nakai, T. Vreven, J. A. Montgomery, Jr., J. E. Peralta, F. Ogliaro, M. Bearpark, J. J. Heyd, E. Brothers, K. N. Kudin, V. N. Staroverov, R. Kobayashi, J. Normand, K. Raghavachari, A. Rendell, J. C. Burant, S. S. Iyengar, J. Tomasi, M. Cossi, N. Rega, J. M. Millam, M. Klene, J. E. Knox, J. B. Cross, V. Bakken, C. Adamo, J. Jaramillo, R. Gomperts, R. E. Stratmann, O. Yazyev, A. J. Austin, R. Cammi, C. Pomelli, J. W. Ochterski, R. L. Martin, K. Morokuma, V. G. Zakrzewski, G. A. Voth, P. Salvador, J. J. Dannenberg, S. Dapprich, A. D. Daniels, Ö. Farkas, J. B. Foresman, J. V. Ortiz, J. Cioslowski, and D. J. Fox, Gaussian, Inc., Wallingford CT, 2009.

**1•+**        **1•**

**Figure S4.** Computed Spin Density isosurfaces (isocontour value 0.025). Positive (blue) zones indicate regions were an excess of electron is present that is the zones were the radical is localized.

**Table S2.** Computed vertical electronic excitations (λ in nm) and oscillator strengths (f in a.u.). Only transitions with relevant intensities are reported and most intense are highlighted in bold face.

| 1 | | 1•+ | | 1• | | 1-QM+ | |
|---|---|---|---|---|---|---|---|
| λ | f | λ | f | λ | f | λ | f |
| **295** | **0.2410** | 490 | 0.0256 | 667 | 0.0459 | 604 | 0.0496 |
| **291** | **0.1895** | **459** | **0.0619** | 653 | 0.0186 | 560 | 0.0234 |
| 287 | 0.0327 | 358 | 0.0325 | 640 | 0.0235 | **461** | **0.3517** |
| 276 | 0.0220 | 353 | 0.0120 | **398** | **0.0674** | **456** | **0.0836** |
| **246** | **0.0751** | 326 | 0.0313 | 390 | 0.0152 | **445** | **0.1182** |
| **245** | **0.2369** | 324 | 0.0129 | **345** | **0.0757** | 435 | 0.0117 |
| | | 318 | 0.0137 | 337 | 0.0203 | 345 | 0.0122 |
| | | 314 | 0.0447 | 311 | 0.0232 | **322** | **0.1968** |
| | | **310** | **0.0873** | **292** | **0.1396** | 310 | 0.0126 |
| | | 304 | 0.0397 | 288 | 0.0306 | 289 | 0.0256 |
| | | 302 | 0.0462 | 286 | 0.0159 | 278 | 0.0222 |
| | | | | 285 | 0.0252 | 277 | 0.0151 |
| | | | | **282** | **0.1106** | 268 | 0.0159 |
| | | | | 278 | 0.0426 | 253 | 0.0353 |
| | | | | 264 | 0.0490 | . | |